Edge detection applied to Cassini images reveals no measurable displacement of Ontario Lacus' margin between 2005 and 2010

Thomas Cornet,[1,2,3] Olivier Bourgeois,[1,2,3] Stéphane Le Mouélic,[1,2,3] Sébastien Rodriguez,[4] Christophe Sotin,[1,2,3,5] Jason W. Barnes,[6] Robert H. Brown,[7] Kevin H. Baines,[5] Bonnie J. Buratti,[5] Roger N. Clark,[8] and Phillip D. Nicholson[9]

Received 5 March 2012; revised 16 May 2012; accepted 2 June 2012; published 18 July 2012.

[1] Ontario Lacus is thus far the largest flat-floored topographic depression of Titan's southern hemisphere interpreted as a permanent or ephemeral lake. From 2005 to 2010, it was imaged several times and at various wavelengths by ISS, VIMS and RADAR instruments onboard Cassini's spacecraft. We analyze the position and uncertainty of Ontario Lacus' margin in all these images using an edge detection method based on image derivation. We find that, given the range of uncertainties in contour locations derived from images, no measurable displacement of Ontario Lacus' margin can be detected between 2005 and 2010 at the actual image spatial resolutions. The discrepancy between this result and previous ones is attributable to differences in (1) the basics behind the methods used, (2) the actual spatial resolutions and contrasts of the available images due to differential atmospheric scattering effects at different wavelengths, and (3) the geomorphological interpretation of contours derived from images acquired at different wavelengths. This lack of measurable displacement in the images suggests that the imaged contour corresponds either (1) to the border of a surface liquid body, provided that potential changes in its extent over five terrestrial years were not sufficiently large to be measured, or (2) to the stationary topographic border between Ontario Lacus' depression and the surrounding alluvial plain. Potential displacements of Ontario Lacus' margin between 2005 and 2010 are thus below the actual resolution of currently available images or have to be sought for within the extent of the topographic depression rather than along its borders.

Citation: Cornet, T., et al. (2012), Edge detection applied to Cassini images reveals no measurable displacement of Ontario Lacus' margin between 2005 and 2010, *J. Geophys. Res.*, *117*, E07005, doi:10.1029/2012JE004073.

1. Introduction

[2] Titan is the only extraterrestrial body known to have stable liquids at its surface. They were first hypothesized to be in the form of a large hydrocarbon ocean mainly composed of ethane, methane and nitrogen [*Lunine et al.*, 1983], prior to the discovery of lakes and seas by the Cassini spacecraft [*Stofan et al.*, 2007]. These lakes have various morphologies, with rounded, lobate, polygonal or dendritic contours, and different radar reflectivity, from bright to dark radar features, potentially indicative of their liquid filling state [*Lopes et al.*, 2007; *Stofan et al.*, 2007; *Hayes et al.*, 2008].

[3] There is a strong hemispherical asymmetry in the lake distribution, with almost all of the surface liquid bodies being currently located in the northern hemisphere that possesses a longer but less intense summer than the southern hemisphere [*Aharonson et al.*, 2009]. In the southern hemisphere, only few lakes appear to be currently liquid-filled. Ontario Lacus (72°S, 180°E, Figure 1) is so far the largest feature interpreted as a surface liquid body [*Brown et al.*, 2008; *Barnes et al.*, 2009; *Turtle et al.*, 2009; *Wye et al.*, 2009; *Hayes et al.*, 2010; *Moriconi et al.*, 2010; *Wall et al.*, 2010; *Hayes et al.*, 2011; *Turtle et al.*, 2011] or as a playa bearing a partial liquid-filling [*Lorenz et al.*, 2010; *Cornet et al.*, 2012].

[4] From a geomorphological point of view, Ontario Lacus (Units A and B, Figure 2) is a shallow, flat-floored, topographic depression, 235 km-long and 75 km-wide; it lies

[1]Université de Nantes, Laboratoire de Planétologie et Géodynamique de Nantes, UMR 6112, Nantes, France.
[2]CNRS, Nantes, France.
[3]OSUNA, Nantes, France.
[4]CEA-Saclay, DSM/IRFU/Service d'Astrophysique, Gif-sur-Yvette, France.
[5]Jet Propulsion Laboratory, California Institute of Technology, Pasadena, California, USA.
[6]Department of Physics, University of Idaho, Moscow, Idaho, USA.
[7]Departments of Planetary Sciences and Astronomy, University of Arizona, Tucson, Arizona, USA.
[8]U. S. Geological Survey, Denver, Colorado, USA.
[9]Department of Astronomy, Cornell University, Ithaca, New York, USA.

Corresponding author: T. Cornet, Université de Nantes, Laboratoire de Planétologie et Géodynamique de Nantes, UMR 6112, 2 rue de la Houssinière, BP92208, F-44000 Nantes, France. (thomas.cornet@univ-nantes.fr)

0148-0227/12/2012JE004073

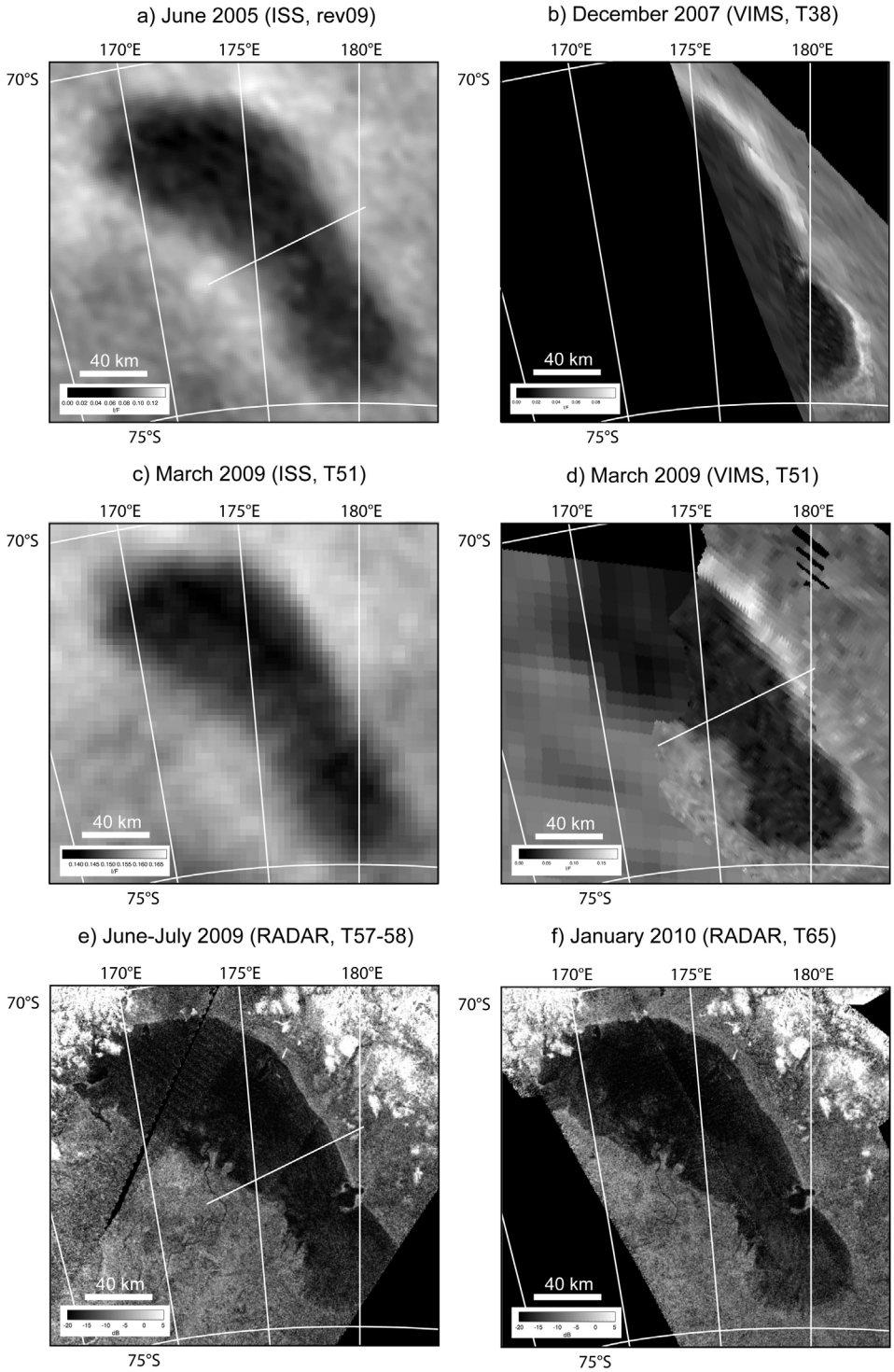

Figure 1. Images of Ontario Lacus acquired by various sensors onboard the Cassini spacecraft (orthographic projection centered at 72° S, 175° E). (a) ISS rev09 (2005), (b) VIMS T38 (2007), (c) ISS T51 (2009), (d) VIMS T51 (2009), (e) RADAR SAR T57–58 (2009), and (f) RADAR SAR T65 (2010). White transverse lines on ISS rev09, VIMS T51 and RADAR T57–58 images indicate the location of cross-sections presented on Figure 3.

in the lowest part of an alluvial plain hundred-km wide (Unit E, Figure 2), which is surrounded by mountain ranges a few hundred-meters high (Unit F, Figure 2) [*Wye et al.*, 2009; *Lorenz et al.*, 2010; *Wall et al.*, 2010; *Cornet et al.*, 2012]. The surface of Ontario Lacus (Units A and B, Figure 2) is extremely smooth at the RADAR wavelength ($\lambda = 2.17$ cm) and has therefore been interpreted as a surface liquid body covering the whole depression floor [*Wye et al.*,

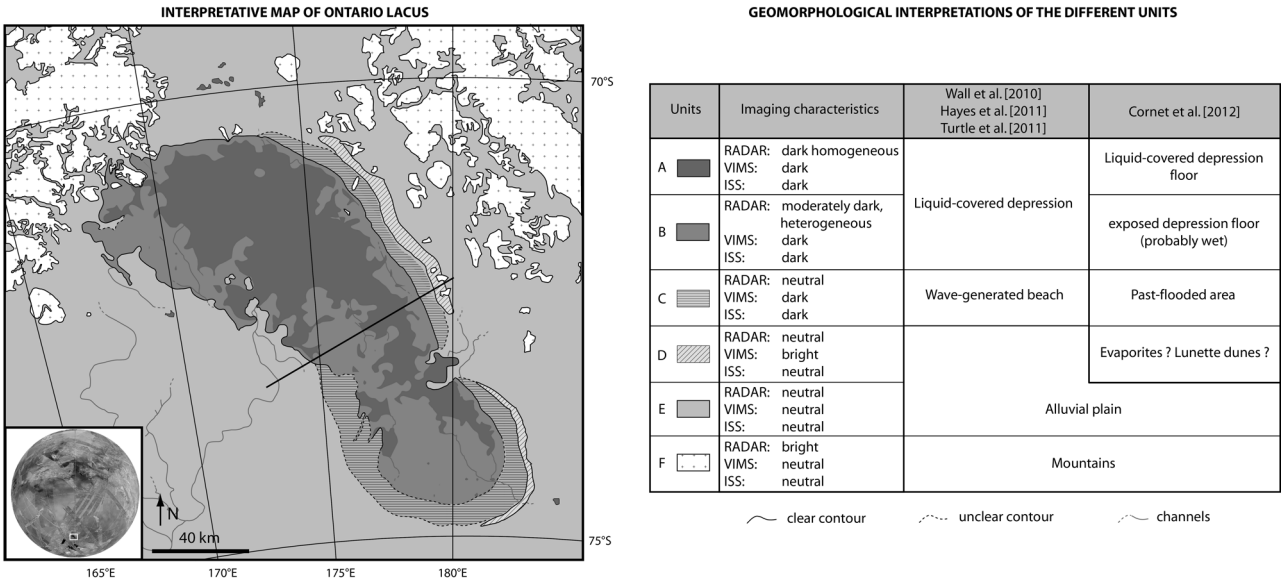

Figure 2. Interpretative map of the Ontario Lacus landsystem, compiled from VIMS, ISS and RADAR data (adapted from *Cornet et al.* [2012], same projection as Figure 1). The global context map of Titan used for location (inset at the bottom left) is an overlap of VIMS and RADAR data in orthographic projection. Current geomorphological interpretations of units comprising the Ontario Lacus landsystem are summarized in the table on the right of the figure. The transverse black line represents the location of cross-sections presented on Figure 3.

2009; *Hayes et al.*, 2010]. This body would be composed of liquid ethane, possibly mixed with other hydrocarboneous components, according to interpretations of the Visual and Infrared Mapping Spectrometer (VIMS) data [*Brown et al.*, 2008; *Moriconi et al.*, 2010] and thermodynamic equilibrium calculations [*Cordier et al.*, 2009]. Changes in the extent of the interpreted liquid-covered area have been reported by comparing Ontario Lacus' contour determined in the Imaging Science Subsystem (ISS) image acquired in 2005 (rev09) with those determined in the RADAR image acquired in 2009 (T57–58) [*Hayes et al.*, 2011], and in the ISS image acquired in 2009 (T51) [*Turtle et al.*, 2011]. By drawing lines of constant recorded radar and infrared signal, these authors determined an average margin recession of about 10 km in the southwestern part of Ontario Lacus.

[5] On the other hand, the presence of channels, seen both in VIMS and RADAR data in the southern part of the depression floor, an area where the radar signal is brighter and more heterogeneous than its northern part, and the persistency of these channels over a 2-years interval (December 2007 to January 2010) has been interpreted as indicating that Ontario Lacus was not entirely covered by liquid hydrocarbons at the time of these observations [*Cornet et al.*, 2012]. According to this interpretation, a smooth solid floor, whose subsurface is probably saturated in liquids, would have been exposed at that time over the southern half of Ontario Lacus (Unit B, Figure 2). Based on this observation and on other geomorphological considerations, *Cornet et al.* [2012] suggested that the closest Earth analogs for the Ontario Lacus landsystem are evaporitic ephemeral lakes that form in shallow flat-floored karstic depressions under semi-arid climates, such as the southern African pans or the Kansas playas [*Goudie and Wells*, 1995; *Miller et al.*, 2010; *Bowen and Johnson*, 2012]. This interpretation is consistent with previous suggestions that ephemeral lakes such as the Racetrack and Bonnie Claire Playas (Death Valley National Park, California) are relevant terrestrial analogues for Ontario Lacus [*Lorenz et al.*, 2010].

[6] If the interpretation of Ontario Lacus as a playa covering the floor of a karstic depression is correct, its margin, which appears as contours on ISS, VIMS and RADAR images, would correspond to the topographic border of the depression rather than to the border of its liquid fill and its location should remain constant over time. Alternatively, if the margin delimits the border of a liquid body, variations of its position between the different data sets could be potentially observed due to evaporation or replenishment of the liquid fill.

[7] The present work thus aims at constraining the location of this margin through time by using a gradient-based image-processing algorithm for automatic edge detection. The method is based on image spatial differentiation, it does not require any previous segmentation or automatic/manual thresholding processes and provides a measure of the uncertainty on locations of detected contours. It is applied to the whole series of data acquired so far on Ontario Lacus by all the imaging sensors of the Cassini spacecraft, to provide a temporal survey of its contour from 2005 to 2010.

2. Data Reduction and Edge Detection Methods

2.1. Data Reduction

[8] We used all the available imagery data sets acquired so far by the Cassini spacecraft over Ontario Lacus. These include data acquired by the Imaging Science Subsystem (ISS) in June 2005 (rev09) and March 2009 (T51), by the Visual and Infrared Mapping Spectrometer (VIMS) in December 2007 (T38) and March 2009 (T51) and by the

Table 1. Characteristics of ISS, VIMS and RADAR Data Sets Acquired on Ontario Lacus From 2005 to 2010

Observation	Incidence (°)	Emission (°)	Phase (°)	Spatial Sampling (km/pixel)	Altitude (km)	Exposure Time (ms)	Imaging Mode	Contrast C_w in Raw/Processed Image
ISS rev09 (June 2005)	50–62	24–38	~64	2.66–2.67	448390	120000	NA IRP0-CB3 FULL	−0.107/−0.321
ISS T51 (March 2009)	66–82	20–44	71–75	2.32–2.44	12295	10000	WA CB3-CL2 SUM4	−0.042/−0.087
VIMS T38 (December 2007)	60–73	45–89	38–42	0.5–2.2	2012–6648	180	HiRes 64 × 32	−0.494/−0.466
VIMS T51 (March 2009)	68–78	13–46	72–74	2.1–17.3	4233–32333	240–320	Normal 32 × 32–64 × 64	−0.610/−0.626
RADAR T57–58 (June–July 2009)	26–44	26–44	-	0.18–0.7	1032–1387	-	SAR	−1.990
RADAR T65 (January 2010)	21–29	21–29	-	0.3–0.5	1109	-	SAR	−1.922

RADAR instrument in June–July 2009 (T57–58) and January 2010 (T65). Table 1 shows the characteristics of each imaging data set over Ontario Lacus' area. Contrast values are calculated with the Weber-Fechner formulae (equation (1)), where C_w is the contrast computed using the normalized difference between the intensity of a given object in the image ($I_{Ontario}$) and the intensity of the background ($I_{background}$), as follows:

$$C_w = \left(I_{Ontario} - I_{background}\right)/I_{background}. \quad (1)$$

[9] ISS data have already been described in *Turtle et al.* [2009] (rev09) and *Turtle et al.* [2011] (T51). ISS images are acquired at 0.93 μm, a wavelength where Titan's surface can be seen but which is subject to intense atmospheric scattering effects due to Titan's haze [*Rodriguez et al.*, 2006]. ISS rev09 data have been acquired with the Narrow Angle Camera (NAC) at lower incidence and phase angles but with similar emission angles than ISS T51 data, acquired with the Wide-angle Camera (WAC). The theoretical spatial sampling of the ISS T51 image is better than that of the ISS rev09 image. However, because of a less favorable viewing geometry at T51, Titan's haze scattering effects are stronger at T51 than at rev09. ISS T51 data therefore appear about 3 times less contrasted than ISS rev09 data (Table 1). ISS images are affected by haze scattering effects, which reduces the actual spatial resolution even after image sharpening [*Porco et al.*, 2004; *Perry et al.*, 2005], compared to that inferred from the ISS spatial sampling. Thus, instead of being equal to, at most, 2 pixels (~5 km), the actual spatial resolution is most probably equal to or greater than 3 pixels (≥7 km) for both ISS images.

[10] VIMS data have been described in *Barnes et al.* [2009] (T38) and *Cornet et al.* [2012] (T51). In this work, we use the images acquired by VIMS in the 5 μm atmospheric window, at wavelengths where Titan's surface can be seen with negligible contribution from haze scattering [*Rodriguez et al.*, 2006]. This is confirmed by the higher contrast of VIMS images compared to that of ISS images (Table 1). VIMS T38 data have been acquired at similar high incidence angles as VIMS T51 data, but with lower phase angles and higher emission angles, making the viewing conditions of VIMS T38 data less favorable (air mass ranging from 3.4 up to 60.7) than those of VIMS T51 data (air mass ranging from 3.7 up to 6.2). The theoretical spatial sampling of the VIMS T38 data is better than that of the VIMS T51 data. Since VIMS images at 5 μm are not affected by Titan's haze scattering, their spatial resolutions can be defined as twice their spatial samplings, thus, at best, 1 km for T38 and 4.2 km for T51.

[11] RADAR SAR data have been described in *Hayes et al.* [2010] and *Wall et al.* [2010] (T57–58 and T65) and *Cornet et al.* [2012] (T65). SAR images are acquired at a 2.17 cm wavelength, and are therefore unaffected by Titan's haze scattering [*Rodriguez et al.*, 2003]. The spatial samplings of the RADAR T57–58 and T65 data are similar, and their actual spatial resolutions depends on volume scattering and are not worst than twice their spatial samplings, thus equal to 0.36–1.4 km and to 0.6–1.0 km for T57–58 and T65, respectively. The computed contrasts of the RADAR images are the best ones among the whole imaging data sets (Table 1).

[12] All the observations are processed, navigated and co-registered according to the procedures described in *Cornet et al.* [2012]. RADAR data are only speckle-noise filtered since they are insensitive to Titan's haze scattering. VIMS data at 5 μm are calibrated and corrected for surface photometry only, since they are not altered by haze scattering. ISS data are calibrated and sharpened using the procedure described in *Porco et al.* [2004] and *Perry et al.* [2005], in order to attenuate the haze blurring effects in the images. The two RADAR data sets are the best spatially correlated images (also highly correlated with the VIMS T51 data) and are taken as references to correct for spatial offsets in the different VIMS and ISS observations [*Cornet et al.*, 2012]. The six corresponding maps are displayed in Figure 1.

2.2. Edge Detection Method

2.2.1. Principle of Edge Detection

[13] In an image, object contours appear as localized changes (i.e., high gradients) in the value of the imaged quantity. On this basis, various edge detection methods have been developed for terrestrial remote-sensing applications and have been applied for civil and geological purposes (detection of channels, shorelines, buildings…) [*Marr and Hildreth*, 1980; *Moore and Waltz*, 1983; *Mather*, 2004]. Common to all these techniques is the principle that an image is formed by gradients or intensity slopes defining boundaries or edges, between high/moderate/low values of the imaged quantity. This quantity is the fraction of sunlight reflected by the surface (I/F, where I is the signal recorded by the instrument and πF the solar incident flux) for ISS and VIMS infrared data, and the radar backscatter cross-section (σ^0) for RADAR SAR data. Edge detectors therefore emphasize the highest gradients between the different regions that form an image and are powerful tools to identify object contours. Edge detection is sensitive to edge orientation (geometry), noise environment and edge structure

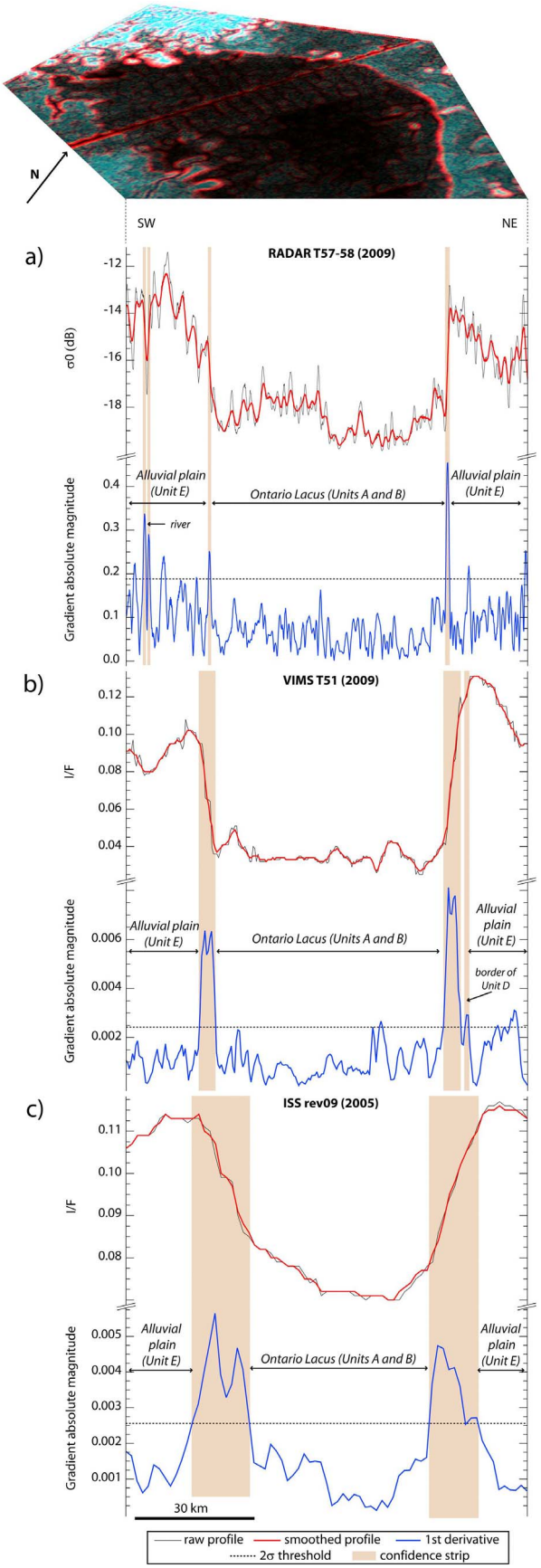

(gradual or step changes in intensity) in the images [*Huertas and Medioni*, 1986; *Mather*, 2004].

[14] The principle of gradient-based edge detection is illustrated in Figure 3 using an example of edge detector based on the computation of the absolute magnitude of the first spatial derivative, applied on spatial profiles of ISS rev09, VIMS T51 and RADAR T57–58 images across Ontario Lacus. The effect of noise can be partly removed by smoothing the image [*Mather*, 2004]. If image smoothing is not intrinsically comprised in the edge detection operator, a smoothing filter must first be applied to reduce small random intensity variations (noise) in images. We applied such a smoothing function to the images prior to the computation of the edge detection operator. This function is a boxcar average smoothing filter, applied with a moving kernel that we fixed equal to 0.5% × 0.5% of the image size in the smaller direction to smooth enough the image without strongly altering its sharpness. The results of this smoothing filter are shown in Figure 3, as thick red lines superimposed on the original I/F and σ^0 profiles (thin black lines).

[15] The absolute magnitude of the first derivatives (blue profiles in Figure 3) of the smoothed profiles were then computed by the finite difference method [*Mather*, 2004]. Peaks in the first derivatives correspond to high gradients (i.e., contours) in the smoothed profiles. By definition, object contours are lines of infinitesimal width that separate regions with contrasting values on images. Contours should thus theoretically appear as peaks of infinitesimal width and infinite height in the first derivative profiles. However, because images are discrete signals composed of pixels of finite width and because atmospheric and volume scattering can respectively produce blurring effects in optical images and increase the noisiness in radar images, contours appear in the first derivative profiles as peaks, the finite heights and finite widths of which depend both on the contrast in the imaged quantity across the contours and on the image resolution. We consider peaks exceeding twice the standard deviation (2σ) of the first derivative as corresponding to significant gradients (i.e., contours) in the smoothed profiles and we take their widths at the 2σ-level as a proxy for their spatial accuracy. This threshold has been chosen because it removes much of the noise while keeping the gradients associated with Ontario Lacus' contour. Peaks can then be mapped in images, as strips of finite width (confidence strips), the sharpness of which directly reflects the spatial accuracy of the detected contours (Figure 3). The width of

Figure 3. Principle of the gradient-based edge detection method. Raw (thin black lines), smoothed (thick red lines) and derivative (blue lines) spatial profiles across (a) RADAR T57–58 σ^0, (b) VIMS T51 I/F and (c) ISS rev09 I/F images over the same region in the southern part of Ontario Lacus. Peaks largely exceeding the 2σ threshold (black horizontal stippled line) in the first derivative profiles are considered as corresponding to significant gradients (i.e., contours) in the smoothed profiles. Peak widths, measured at the 2σ level, are taken as a proxy for the accuracy of contour locations and can be converted into confidence strips (pink vertical bars). Confidence strips appear in red in the RGB color composite above the RADAR profile (R: derived image, G: raw image, B: smoothed image).

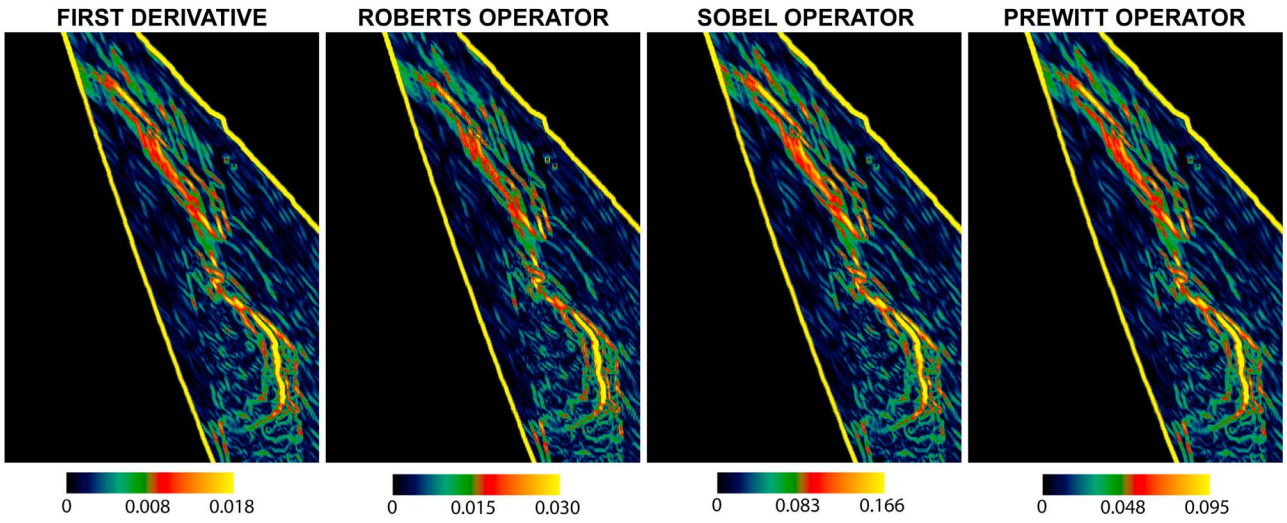

Figure 4. Comparison of contours detected by the gradient method and by the Sobel/Roberts/Prewitt edge detection operators on the VIMS T38 image at 5 μm. Pixels in each panel are color-coded according to the value of the corresponding operator. All these operators give similar edge detections (Table 2).

confidence strips associated with Ontario Lacus' contour in Figure 3 are on the order of the image actual spatial resolutions: approximately 1.4 km for the RADAR profile, 4.1 km for the VIMS profile, and 12 km for the ISS profile.

2.2.2. Sensitivity of Contours to the Edge Detection Method

[16] A series of classical edge detection methods have been tested independently on the images of Ontario Lacus to ensure that the location and sharpness of the detected contours are not biased by the method. These edge detectors include the gradient (or first order derivative) method [*Mather*, 2004] as well as the Sobel [*Sobel*, 1970], Prewitt [*Prewitt*, 1970; *Gonzalez and Woods*, 1992] and Roberts [*Roberts*, 1965; *Shaw et al.*, 1982] operators. Descriptions and comparisons of these detection methods are available in *Maini and Aggarwal* [2009] and in *Juneja and Singh Sandhu* [2009]. The gradient method is based on the detection of maxima and minima in the first derivative of an image in x and y directions. We computed the first derivative by the method of finite differences and kept the absolute magnitude of the gradients [*Mather*, 2004].

[17] The Sobel edge operator approximates the absolute magnitude of the gradient with a smoothing procedure, using a pair of 3×3 convolution kernels horizontally and vertically sensitive to the edges. The Roberts edge operator is similar to the Sobel edge operator and approximates the absolute magnitude of the gradient using a pair of 2×2 convolution kernels designed to get a maximum sensitivity to edges in the diagonals directions rather than in the x and y directions. The Prewitt operator is also a variant of the Sobel operator, with the use of a pair of 3×3 convolution kernels to detect the gradient in x and y directions, but is theoretically efficient only on well-contrasted noiseless images.

[18] For all the images used in this study, there is a high coherence in the location and sharpness of the detected contours, whatever the method used. To illustrate this coherence, the results of all the edge detection methods applied to the VIMS T38 5 μm image are displayed in Figure 4. Table 2 shows the correlation coefficients between the gradient-based edge detector and the Sobel, Roberts and Prewitt edge detectors. Given this high correlation between the different edge detectors (greater than 97%), we keep the simplest method, the gradient method combined with the smoothing filter described above, to detect contours in Ontario Lacus' images from 2005 to 2010.

3. Cross-Comparison of Detected Contours

[19] The results of the edge detection using the gradient-based method on all images are displayed in Figure 5. The detected contours exceeding the 2σ-level are superimposed in Figure 6, with their respective confidence strips. Ontario Lacus' contours derived from the RADAR T57–58 (June–July 2009, Figure 5e) and T65 (January 2010, Figure 5f) images match so perfectly that they are undistinguishable from each other. They embrace Units A and B (Figure 2), interpreted either collectively as an entire liquid fill of Ontario Lacus [*Wall et al.*, 2010; *Hayes et al.*, 2011], or respectively as the liquid-covered and non liquid-covered parts of the depression floor [*Cornet et al.*, 2012]. Significantly, no distinct contour is detected along the southernmost border of Ontario Lacus on RADAR images, which indicates that the transition in physical properties between Unit B and the surrounding units C and E, comprising the alluvial plain (Figure 2), is progressive in this region. This progressive transition is consistent with the interpretation

Table 2. Correlation Coefficients Between T38 5 μm Images Resulting From the Several Edge Detection Operators Shown in Figure 4

Edge Detectors	Gradient	Roberts	Sobel	Prewitt
Gradient	1.0000	0.9811	0.9981	1.0000
Roberts	0.9811	1.0000	0.9700	0.9819
Sobel	0.9981	0.9700	1.0000	0.9985
Prewitt	1.0000	0.9819	0.9985	1.0000

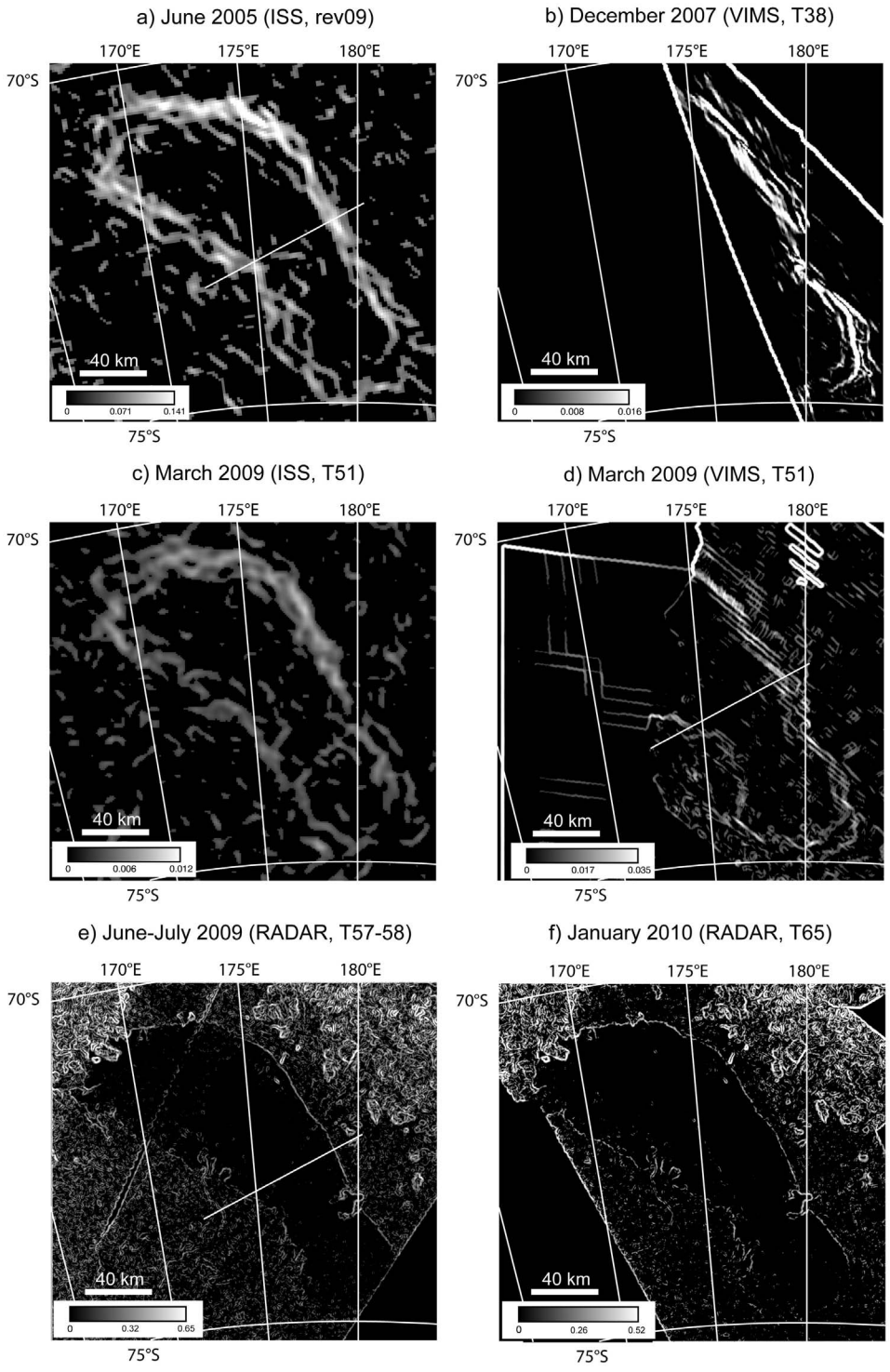

Figure 5. Contours detected by the gradient method on ISS, VIMS and RADAR images of Ontario Lacus (same projection as Figure 1). Each image is shaded according to the value of its first derivative. Pixels with values lower than the 2σ segmentation threshold are left black, thus underlying the detected contours and their confidence strips. (a) ISS rev09 (2005), (b) VIMS T38 (2007), (c) .ISS T51 (2009), (d) VIMS T51 (2009), (e) RADAR SAR T57–58 (2009), and (f) RADAR SAR T65 (2010). White transverse lines on ISS rev09, VIMS T51 and RADAR T57–58 images indicate the location of cross-sections shown on Figure 3.

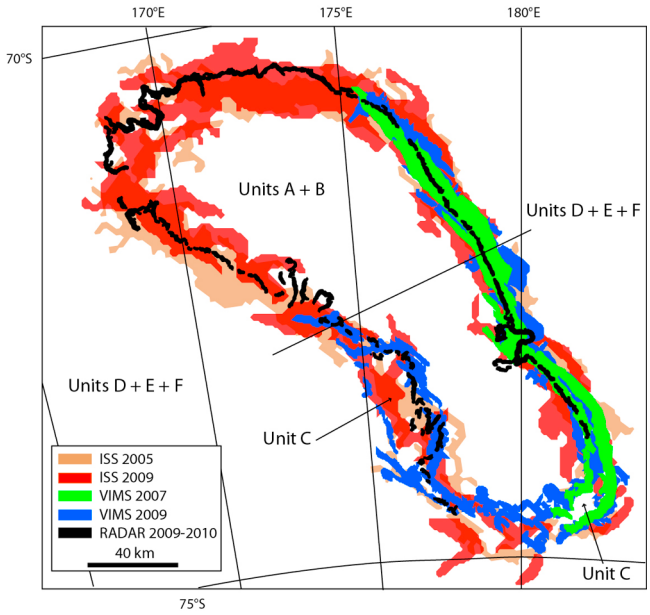

Figure 6. Overlapping of Ontario Lacus' contours detected from each data set (same projection as Figure 1). Each contour is drawn as a strip of finite width (confidence strip) reflecting its spatial accuracy. No measurable difference (i.e., no spatial offset greater than the confidence strips) is found in the location of the determined contours except at the southwest, where Unit C is resolved in VIMS but barely detectable in ISS images and unseen in the RADAR images. Uppercase letters refer to geomorphological units defined in Figure 2. The thin black transverse line indicates the location of the cross-sections shown in Figure 3.

that a liquid layer covers Ontario Lacus' Units A and B and deepens with distance from the shoreline [*Hayes et al.*, 2010], provided that the liquid/solid surface transition is barely detected with the RADAR in this region. Alternatively, it is also consistent with the interpretation that the solid depression floor is exposed in the southern half of Ontario Lacus (Unit B) [*Cornet et al.*, 2012] and merges progressively southwards with the surrounding alluvial plain (Units C and E).

[20] The contours derived from the VIMS T38 (December 2007) and VIMS T51 (March 2009) images at 5 μm (Figures 5b and 5d) are highly correlated with those derived from the RADAR images, though their confidence strips are wider. They also embrace Units A and B (Figure 2). The outer contour of Unit C (Figure 2), which surrounds the southern part of Ontario Lacus, is also distinctively detected in VIMS images. Unit C has been interpreted as a portion of the alluvial plain that was flooded at some time in the past [*Barnes et al.*, 2009; *Cornet et al.*, 2012], which is also consistent with the interpretation that the floor of Ontario Lacus merges progressively southwards with the alluvial plain.

[21] The first-derivative images computed from both ISS images (ISS rev09 and ISS T51) display multiple apparent contours that are either parallel to or crosscut each other (Figures 5a and 5c). The origin of these multiple contours resides in textural variations, visible as a flocculent texture and produced by medium-spatial-wavelength noise covering the whole extent of the original images (Figures 1a and 1c). Some of these multiple contours are thus artifacts due medium-spatial-wavelength noise superimposed on real contours.

[22] The main contour derived from the ISS T51 (March 2009) image embraces Units A and B (Figures 2 and 5c). It correlates well with that derived from the VIMS T51 (Figure 5d) image, acquired at the same date, though with a wider confidence strip (Figure 6). It correlates also with contours derived from the VIMS T38 image (Figure 5b) acquired earlier and with the RADAR T57–58 (Figure 5e) and RADAR T65 (Figure 5f) images acquired later. The only noticeable mismatch between contours derived from ISS T51 and VIMS T51 images is located along the southwestern border of Ontario Lacus, where the ISS T51 contour stretches across Unit C (Figure 6). This mismatch between contours derived from two images acquired at the same date is perhaps an artifact due the medium-spatial-wavelength noise described above, in addition to the very low contrast of the ISS image (Table 1). Other possible reasons for this mismatch are discussed in section 4. A second contour parallels the main contour along the southeastern border of Ontario Lacus (Figure 5c). This second contour apparently correlates with the outer contour of Unit C as seen in the VIMS T38 and VIMS T51 images. However, by contrast with the VIMS T51 observation, it is not detected on the ISS T51 image along the southwestern border of Ontario Lacus. Therefore we cannot assess whether this second contour indeed corresponds to the outer border of Unit C or rather to an artifact due to medium-wavelength noise and reduced contrast of the ISS T51 image.

[23] The main contour derived from the ISS rev09 (June 2005) image embraces Units A and B (Figures 2 and 5a). It correlates well with contours derived from all other images (Figure 6). This contour however splits into multiple apparent contours along the southeastern and southwestern borders of Ontario Lacus (Figure 5a). The outermost contour is well defined, nearly continuous, and apparently correlates with the outer border of Unit C as seen in VIMS images (Figure 6). On the other hand, the innermost contour apparently correlates with the inner border of Unit C, but is difficult to reconcile over its whole extent. More specifically, three apparent contours are detected along the southwestern border of Ontario Lacus (Figure 6). It is therefore difficult to determine whether these multiple apparent contours indeed correspond to the borders of Unit C or rather to artifacts due to medium-wavelength noise and poor contrast of the ISS rev09 image (Table 1).

4. Discussion

[24] On the basis of the geographic match between contours derived from all images, and given the width of their respective confidence strips, the medium-spatial wavelength noise and the poor contrast of ISS images, we cannot conclude that measurable displacements of Ontario Lacus' margin occurred between June 2005 and January 2010. Most significantly, the contours derived from the images with the best actual spatial resolution (RADAR T57–58 and T65) perfectly match with one another (Figure 6). This means that Ontario Lacus' margin has not moved by more than 1.4 km (the average width of the confidence strip of contours

derived from RADAR images) between June 2009 and January 2010. These contours match also with those derived from VIMS T38 and T51 images, indicating that Ontario Lacus' margin has not moved by more than 4.2 km (the average width of the confidence strip of contours derived from VIMS images) between 2007 and 2010. Over a longer timescale, no displacement larger than 7 to 10.5 km (the average width of the confidence strip of contours derived from ISS images) can be determined between 2005 and 2010. Any potential displacement smaller than these values is below the actual resolution of currently available images. This lack of measurable displacements is consistent with the interpretation that the imaged contour corresponds either (1) to the border of a surface liquid body, provided that potential changes in the extent of this liquid body were no sufficiently large to be measured on currently available images, or (2) to the stationary topographic margin of a depression [*Cornet et al.*, 2012].

[25] This lack of measurable changes is not in agreement with previous analyses by *Hayes et al.* [2011] and *Turtle et al.* [2011], who argued respectively that contour displacements of 10–20 km and 9–11 km can be detected along the southwestern border of Ontario Lacus between 2005 and 2009. *Hayes et al.* [2011] detected these changes by comparing ISS rev09 (2005) and RADAR T57–58 (2009) images, while *Turtle et al.* [2011] used a comparison between ISS rev09 (2005) and ISS T51 (2009) images. Several reasons for this disagreement can be invoked, including (1) differences in the basics behind the methods used, (2) differences in the actual resolution and contrast of ISS, VIMS and RADAR images due to differential atmospheric scattering effects at different wavelengths, and (3) differences in the geomorphological interpretation of contours derived from images acquired at different wavelengths.

4.1. Influence of the Detection Method

[26] *Hayes et al.* [2011] determined the position of the margin of Ontario Lacus in the RADAR T57–58 image by drawing an isocontour corresponding to the sharp transition in σ^0 between the dark interior and the grayish exterior of Ontario Lacus. This RADAR contour is sharp because (1) the image has a high spatial sampling of ~300 m/pixel, (2) microwaves are not sensitive to atmospheric scattering, and (3) the different surface units are very contrasted at the radar wavelength. The position of the contour on the ISS rev09 image was determined by *Hayes et al.* [2011] by drawing a line of constant I/F value that matches the overall shape of Ontario Lacus. The contours were thus defined as lines joining pixels of constant values in both kinds of images, and no confidence strips were associated to their locations.

[27] *Turtle et al.* [2011] compared the position of the contour of Ontario Lacus between the ISS images acquired in June 2005 (rev09) and March 2009 (T51). They detected the contours of the depression using a segmentation process. An average value between the pixels on each side of Ontario Lacus and those inside of Ontario Lacus was used as a threshold to map the contour. The sensitivity of the contour location to small variations in the threshold value was tested to assess the accuracy.

[28] Fundamental behind the methods used by *Hayes et al.* [2011] and *Turtle et al.* [2011] is the assumption that an object contour in an image is defined by a constant value of the imaged quantity, which works best when this quantity remains constant over the whole extent of a given unit and significantly changes from one unit to the other. Intrinsic surface variations or extrinsic causes (illumination, viewing conditions) can however produce internal variations of the imaged quantity within a given unit. This is particularly true when the calibration process is heavy in order to remove signals not related to the characteristics of the surface such as atmospheric scattering for optical images. To overcome this drawback, a number of robust and conventional edge detection techniques (such as the gradient-based edge detection used here) have been developed [*Mather*, 2004; *Maini and Aggarwal*, 2009; *Juneja and Singh Sandhu*, 2009]. All of them rely on the assumption that object contours are defined by localized gradients in the imaged quantity rather than by the value of this quantity. With these methods, objects are thus not recognized by their absolute reflectivity values, but by their contrast with each other. This fundamental difference in the definition of objects in images partly explains the discrepancy between our results and those of *Hayes et al.* [2011] and *Turtle et al.* [2011]. In addition, an advantage of gradient-based edge detection methods is that, as explained in section 2.2, they intrinsically provide quantitative estimates of uncertainties in contour locations. These can be mapped in the form of confidence strips, which directly depends on the actual resolution and contrast of the images (Figure 3).

4.2. Effect of Titan's Atmospheric Scattering on Contour Detection

[29] At wavelengths shorter than 5 μm, Titan's atmospheric scattering strongly reduces the contrast and alters the spatial resolution of images (section 2.1). This effect, due to both molecular and haze scattering by small particles (typically less than 1 μm in radius), mostly depends on the viewing geometry and on the wavelength: it is particularly strong at wavelengths shorter than ~3 μm, and becomes negligible at longer wavelengths [*Rodriguez et al.*, 2006]. ISS images at 0.93 μm are thus particularly sensitive to Titan's atmospheric scattering while 5-μm VIMS and 2.2-cm RADAR images can be considered free of atmospheric scattering effects. As a consequence, ISS images are significantly blurred by the atmosphere, which results in reduced contrast (Table 1) and poor actual spatial resolution (see section 2.1) compared to those of RADAR and VIMS images, even after image sharpening processes have been applied [*Porco et al.*, 2004; *Perry et al.*, 2005]. Contours derived from these images are therefore less sharp than contours derived from RADAR and VIMS images (Figures 5 and 6), which results in wider confidence strips.

[30] This scattering effect, combined with other causes discussed in sections 4.1 and 4.3, explains most of the discrepancy between our results and those of *Hayes et al.* [2011] and *Turtle et al.* [2011]. This is particularly well illustrated by comparing contours derived from ISS T51 and VIMS T51 images, which were acquired at the same date, with those derived from RADAR images acquired 3–4 (T57–58) and 10 (T65) months later (Figures 5 and 6). Whereas Ontario Lacus' contour derived from the VIMS T51 image perfectly matches the contour derived from RADAR images, the contour derived from the ISS T51 image differs slightly in the southwestern part of Ontario

Lacus (Figure 6). Since (1) no change in the infrared spectral behavior has been documented so far for Ontario Lacus' interior, (2) VIMS data require much less processing at 5 μm than ISS does at 0.93 μm due to the atmospheric scattering effects present in ISS images, and (3) the shape of Ontario Lacus' contour is identical in VIMS and RADAR data, we suspect that the difference in shape between ISS and VIMS images acquired during the same flyby (T51) is an artifact due to atmospheric scattering on the ISS T51 image. This interpretation is strengthened by the fact that it is not the case for the ISS rev09 image, the viewing geometry of which is more favorable than that of the ISS T51 image (section 2.1), and therefore less prone to atmospheric scattering. The contrast in ISS rev09 image, weaker but of the same order as that in the VIMS T51 image, is thus stronger than the contrast in the ISS T51 image, which may also explain why the outer contour of Unit C is not seen in the latter image while it is detected in the former images.

4.3. Geomorphological Interpretation of Detected Contours

[31] The Ontario Lacus landsystem comprises different geomorphological units, which differ in their infrared and/or microwave signatures (Figures 1 and 2). Of particular interest to this study are the following units.

[32] 1. Units A and B are located in the Ontario Lacus topographic depression [*Wye et al.*, 2009; *Cornet et al.*, 2012]. These units have been interpreted either (1) collectively as a surface liquid body covering entirely the depression floor [*Brown et al.*, 2008; *Wye et al.*, 2009; *Wall et al.*, 2010; *Hayes et al.*, 2010], or (2) respectively as the liquid-covered and exposed parts of the depression floor [*Cornet et al.*, 2012].

[33] 2. Unit E surrounds the topographic depression and has been interpreted as an alluvial plain [*Lorenz et al.*, 2010; *Wall et al.*, 2010; *Cornet et al.*, 2012].

[34] 3. Unit C is a curved strip located between the topographic depression and the alluvial plain along the southern and eastern margins of Ontario Lacus (Figure 2). It has been interpreted either (1) as a part of the liquid body that covers the depression floor [*Hayes et al.*, 2011; *Turtle et al.*, 2011], or (2) as a part of the alluvial plain that was flooded at some time in the past [*Barnes et al.*, 2009; *Cornet et al.*, 2012].

[35] At optical wavelengths, the brightness of Unit C is intermediate between that of Units A and B on one side, and that of Unit E on the other side (Figure 1). Therefore, it is barely resolved in ISS images, because of the low contrast and poor actual resolution inherent to images acquired at short wavelengths through Titan's atmosphere. This is well illustrated by the fact that the inner and outer contours of Unit C are poorly defined and lack continuity when edge detection is applied to ISS images (Figures 5a and 5c). On the other hand, Unit C is visible in VIMS data thanks to its specific spectral properties [*Barnes et al.*, 2009; *Cornet et al.*, 2012] and its inner and outer contours are resolved when edge detection is applied to VIMS images (Figures 5b, 5d, and 6). Unit C is not differentiated from Unit E in RADAR images (Figure 1), which suggests that its physical properties with respect to microwaves are similar to those of the alluvial plain.

[36] In analyzes of ISS images performed by *Hayes et al.* [2011] and *Turtle et al.* [2011], Unit C was considered as a part of the Ontario Lacus liquid fill. However, the good spatial correlation between VIMS T51 and RADAR T57-58-65 data, along with the altimetry data given by the T49 RADAR altimetric profile, indicates that Unit C is located outside of the Ontario Lacus topographic depression [*Cornet et al.*, 2012] and therefore cannot be part of its current liquid fill. Thus, poor visibility of Unit C on ISS images, due to its poor contrast with respect to adjacent units, is an important reason for the discrepancy between our results and those of previous workers.

5. Conclusion

[37] We mapped the contour of Ontario Lacus in images obtained between 2005 and 2010 using a conventional edge detection method based on the computation of spatial gradients in images. This method provides quantitative estimates, in the form of confidence strips, of the spatial accuracy of the detected contours. We applied this method to all the images of Ontario Lacus thus far acquired by the Cassini ISS, VIMS and RADAR instruments. We find that no measurable changes in the shape of this contour can be highlighted between 2005 and 2010 at the actual spatial resolutions of the observations. Differences in the fundamental assumptions lying behind the contour detection methods and in estimates of errors on locations of detected contours explain much of the discrepancy between our results and those of previous analyses [*Hayes et al.*, 2011; *Turtle et al.*, 2011], in addition to atmospheric scattering effects that are responsible for large uncertainties in the location of contours derived from ISS images. Interpretation of the distinct geomorphological units has also strong consequences on the change detection.

[38] The lack of measurable displacements means that potential displacements of Ontario Lacus' margin cannot be detected at the spatial resolution of the available data sets. This lack of measurable displacements is consistent with the interpretation that the imaged contour is the border of a surface liquid body [*Brown et al.*, 2008; *Hayes et al.*, 2010; *Wall et al.*, 2010], provided that the extent of this liquid body has not changed significantly between 2005 and 2010. This would imply that the balance between evaporation and precipitation was not sufficiently in favor of one or the other at the time of the observations to produce measurable changes in the extent of the surface liquid body. This is consistent with recent modeling results of a 3D GCM [*Schneider et al.*, 2012], which indicate potential replenishment of Ontario Lacus with methane between 1997 and 2007 (Evaporation – Precipitation < 0) and slow evaporation of this methane since 2007 (Evaporation – Precipitation ≥ 0), with an absence of additional precipitations until around 2027. The lack of measurable displacement of the margin is also consistent with the presence of ethane in Ontario Lacus, which has been detected from VIMS data [*Brown et al.*, 2008] and which would reduce the evaporation rate [*Mitri et al.*, 2007].

[39] Alternatively, the lack of measurable displacement of Ontario Lacus' margin is consistent with the interpretation that the imaged contour actually represents the topographic margin of a shallow flat-floored depression [*Lorenz et al.*, 2010; *Cornet et al.*, 2012] rather than the border of a shallowing liquid fill [*Wye et al.*, 2009; *Hayes et al.*, 2010; *Wall*

et al., 2010]. If this alternative interpretation is correct, potential temporal changes in the extent of the liquid fill would have to be sought for on the floor of the depression (e.g., at the border between Units A and B, Figure 2) rather than along its margin.

[40] The Ontario Lacus region is currently progressing into the dark winter season and after 2012 will remain in the dark up to the end of the Cassini Solstice mission in 2017. Thus, no further VIMS or ISS imaging will be possible during the mission. The potential acquisition of new RADAR data would allow further measurements of the temporal behavior of Ontario Lacus, before awaiting the next, as yet unfunded, Titan mission.

[41] **Acknowledgments.** The authors appreciate financial support provided by the Centre National d'Etudes Spatiales (CNES, France), the Institut National des Sciences de l'Univers (INSU Programme National de Planétologie, Programme Reliefs, France) and the Agence Nationale de la Recherche (project ANR-07-BLAN-0127 "Exoclimats," France). Part of this work has been performed at the Jet Propulsion Laboratory, California Institute of Technology under contract with NASA. C.S. acknowledges support by NASA Astrobiology Institute. We thank Ellen Stofan and an anonymous reviewer for their effort in reviewing a preliminary version of the manuscript and for helping us clarify a number of important points.

References

Aharonson, O., A. G. Hayes, J. I. Lunine, R. D. Lorenz, M. D. Allison, and C. Elachi (2009), An asymetric distribution of lakes on Titan as a possible consequence of orbital forcing, *Nat. Geosci.*, *2*, 851–854, doi:10.1038/ngeo698.

Barnes, J. W., et al. (2009), Shoreline features of Titan's Ontario Lacus from Cassini/VIMS observations, *Icarus*, *201*(1), 217–225, doi:10.1016/j.icarus.2008.12.028.

Bowen, M. W., and W. C. Johnson (2012), Late quaternary environmental reconstructions of playa-lunette system evolution on the central High Plains of Kansas, United States, *Geol. Soc. Am. Bull.*, *124*(1), 146–161, doi:10.1130/B30382.1.

Brown, R. H., L. A. Soderblom, J. M. Soderblom, R. N. Clark, R. Jaumann, J. W. Barnes, C. Sotin, B. Buratti, K. H. Baines, and P. D. Nicholson (2008), The identification of liquid ethane in Titan's Ontario Lacus, *Nature*, *454*, 607–610, doi:10.1038/nature07100.

Cordier, D., O. Mousis, J. I. Lunine, P. Lavvas, and V. Vuitton (2009), An estimate of the chemical composition of Titan's lakes, *Astrophys. J.*, *707*, L128–L131, doi:10.1088/0004-637X/707/2/L128.

Cornet, T., et al. (2012), Geomorphological significance of Ontario Lacus on Titan: Integrated interpretation of Cassini VIMS, ISS and RADAR data and comparison with the Etosha Pan (Namibia), *Icarus*, *218*(2), 788–806, doi:10.1016/j.icarus.2012.01.013.

Gonzalez, R. C., and R. E. Woods (1992), *Digital Image Processing*, Addison-Wesley, Reading, Mass.

Goudie, A. S., and G. L. Wells (1995), The nature, distribution and formation of pans in arid zones, *Earth Sci. Rev.*, *38*, 1–69, doi:10.1016/0012-8252(94)00066-6.

Hayes, A., et al. (2008), Hydrocarbon lakes on Titan: Distribution and interaction with an isotropic porous regolith, *Geophys. Res. Lett.*, *35*, L09204, doi:10.1029/2008GL033409.

Hayes, A. G., et al. (2010), Bathymetry and absorptivity of Titan's Ontario Lacus, *J. Geophys. Res.*, *115*, E09009, doi:10.1029/2009JE003557.

Hayes, A. G., et al. (2011), Transient surface liquid in Titan's polar regions from Cassini, *Icarus*, *211*(1), 655–671, doi:10.1016/j.icarus.2010.08.017.

Huertas, A., and G. Medioni (1986), Detection of intensity changes with sub-pixel accuracy using Laplacian-Gaussian masks, *IEEE Trans. Pattern Anal. Mach. Intell.*, *PAMI-8*(5), 651–664, doi:10.1109/TPAMI.1986.4767838.

Juneja, M., and P. Singh Sandhu (2009), Performance evaluation of edge detection techniques for images in spatial domain, *Int. J. Comput. Theory Eng.*, *1*(5), 614–621.

Lopes, R. M. C., et al. (2007), The lakes and seas of Titan, *Eos Trans. AGU*, *88*(51), 569–576, doi:10.1029/2007EO510001.

Lorenz, R. D., B. Jackson, and A. Hayes (2010), Racetrack and Bonnie Claire: Southwestern US playa lakes as analogs for Ontario Lacus, Titan, *Planet. Space Sci.*, *58*(4), 724–731, doi:10.1016/j.pss.2009.05.012.

Lunine, J. I., D. J. Stevenson, and Y. L. Yung (1983), Ethane ocean on Titan, *Science*, *222*(4629), 1229–1230, doi:10.1126/science.222.4629.1229.

Maini, R., and H. Aggarwal (2009), Study and comparison of various edge detection techniques, *Int. J. Image Proc.*, *3*(1), 1–11.

Marr, D., and E. Hildreth (1980), Theory of edge detection, *Proc. R. Soc. London, Ser. B*, *207*, 187–217, doi:10.1098/rspb.1980.0020.

Mather, P. M. (2004), *Computer Processing of Remotely Sensed Images, An Introduction*, 3rd ed., 324 pp., Jon Wiley, Hoboken, N. J.

Miller, R. M., M. Pickford, and B. Senut (2010), The geology, palaeontology and evolution of the Etosha Pan, Namibia: Implications for terminal Kalahari deposition, *S. Afr. J. Geol.*, *113*(3), 307–334, doi:10.2113/gssajg.113.3.307.

Mitri, G., A. P. Showman, J. I. Lunine, and R. D. Lorenz (2007), Hydrocarbon lakes on Titan, *Icarus*, *186*(2), 385–394, doi:10.1016/j.icarus.2006.09.004.

Moore, G. K., and F. A. Waltz (1983), Objective procedures for lineament enhancement and extraction, *Photogramm. Eng. Remote Sens.*, *49*, 641–647.

Moriconi, M. L., J. I. Lunine, A. Adriani, E. D'Aversa, A. Negrao, G. Filacchione, and A. Coradini (2010), Characterization of Titan's Ontario Lacus region from Cassini/VIMS observations, *Icarus*, *210*(2), 823–831, doi:10.1016/j.icarus.2010.07.023.

Perry, J., A. McEwen, S. Fussner, E. Turtle, R. West, C. Porco, B. Knowles, and D. Dawson, and the Cassini ISS Team (2005), Processing ISS images of Titan's surface, *Lunar Planet. Sci.*, *XXXVI*, Abstract 2312.

Porco, C. C., et al. (2004), Cassini imaging science: Instrument characteristics and anticipated scientific investigations at Saturn, *Space Sci. Rev.*, *115*, 363–497, doi:10.1007/s11214-004-1456-7.

Prewitt, J. (1970), *Object Enhancement and Extraction*, edited by B. Lipkin and A. Rosenfeld, Academic, New York.

Roberts, L. G. (1965), Machine perception of three-dimensional solids, in *Optical and ElectroOptical Information Processing*, edited by J. P. Tippett, pp. 159–197, MIT Press, Cambridge, Mass.

Rodriguez, S., P. Paillou, M. Dobrijevic, G. Ruffié, P. Coll, J. M. Bernard, and P. Encrenaz (2003), Impact of aerosols in Titan's atmosphere on the CASSINI radar experiment, *Icarus*, *164*, 213–227, doi:10.1016/S0019-1035(03)00125-8.

Rodriguez, S., et al. (2006), Cassini/VIMS hyperspectral observations of the Huygens landing site on Titan, *Planet. Space Sci.*, *54*, 1510–1523, doi:10.1016/j.pss.2006.06.016.

Schneider, T., S. D. B. Graves, E. L. Schaller, and M. E. Brown (2012), Polar methane accumulation and rainstorms on Titan from simulations of the methane cycle, *Nature*, *481*, 58–61, doi:10.1038/nature10666.

Shaw, R., L. Sowers, and E. Sanchez (1982), A comparative study of linear and non-linear edge finding techniques for Landsat multispectral data, in *Proceedings of the Pecora VII Symposium, Sioux Falls, South Dakota*, edited by B. F. Richason Jr., pp. 529–542, Am. Soc. of Photogramm. and Remote Sens., Falls Church, Va.

Sobel, I. (1970), Camera models and perception, PhD thesis, Stanford Univ., Stanford, Calif.

Stofan, E. R., et al. (2007), The lakes of Titan, *Nature*, *445*, 61–64, doi:10.1038/nature05438.

Turtle, E. P., J. E. Perry, A. S. McEwen, A. D. DelGenio, J. Barbara, R. A. West, D. D. Dawson, and C. C. Porco (2009), Cassini imaging of Titan's high-latitude lakes, clouds, and south-polar surface changes, *Geophys. Res. Lett.*, *36*, L02204, doi:10.1029/2008GL036186.

Turtle, E. P., J. E. Perry, A. G. Hayes, and A. S. McEwen (2011), Shoreline retreat at Titan's Ontario Lacus and Arrakis Planitia from Cassini Imaging Science Subsystem observations, *Icarus*, *212*(2), 957–959, doi:10.1016/j.icarus.2011.02.005.

Wall, S., et al. (2010), Active shoreline of Ontario Lacus, Titan: A morphological study of the lake and its surroundings, *Geophys. Res. Lett.*, *37*, L05202, doi:10.1029/2009GL041821.

Wye, L. C., H. A. Zebker, and R. D. Lorenz (2009), Smoothness of Titan's Ontario Lacus: Constraints from Cassini RADAR specular reflexion data, *Geophys. Res. Lett.*, *36*, L16201, doi:10.1029/2009GL039588.